COMPARING THE SEMI-LAGRANGIAN SPECTRAL AND GRID-POINT VERSIONS OF THE *HIRLAM* FORECAST MODEL.

A McDonald,
Irish Meteorological Service,
Dublin, Ireland.

Nils Gustafsson,
Swedish Meteorological and Hydrological Institute,
Norrköping, Sweden.

1. INTRODUCTION

The Nordic countries, the Netherlands, and Ireland have combined in a cooperative research effort to develop, maintain, and improve a fully operational suite of programs for producing accurate short range forecasts (out to 48h). They have adopted the name ' the HIRLAM group' (from HIgh Resolution Limited Area Modelling). As part of that research effort the group have been investigating both spectral and grid-point discretization in space and both Eulerian and semi-Lagrangian discretization in time. In this talk we wish to report on the semi-Lagrangian aspects of this work.

Initial progress on the grid-point approach was reported by Kaas (1987) who developed a three time level two-dimensional semi-Lagrangian model which used sigma coordinates for the vertical discretization. McDonald and Haugen (1992), hereinafter called MH1, extended the semi-Lagrangian scheme to three dimensions and added the option of using two levels rather than three to discretize in time. Later, they extended the model to allow for the hybrid coordinate to be used for vertical discretization; see McDonald and Haugen (1993), hereinafter called MH2.

At the same time the spectral approach was investigated first by Machenhauer and Haugen (1987 and 1993), who modelled the shallow water equations with a three time level semi-Lagrangian scheme. This was extended to the full three dimensional primitive equations by Gustafsson (1991), and subsequently an improved two time level version was reported, also by Gustafsson (1995), from here on referred to as G95.

Other groups were simultaneously developing similar models; see Staniforth and Coté (1991) for an excellent review. For an update of subsequent progress, in grid-point space, see Moorthi, Higgins, and Bates (1994) and references therein , and in spectral space see Ritchie, et al. (1994) and references therein.

The model equations are described in section 2, along with a discussion of how the non-periodicity of the boundaries is dealt with in the spectral model. Also, we contrast two different ways of updating the vertical velocity. In section 3 we show some forecasts from both models and discuss their implications. In section 4 we discuss the relative merits of the spectral and grid point approaches to numerical weather prediction.

2. THE MODEL EQUATIONS.

Unless otherwise stated the notation used in this section is conventional. See the appendix for definitions of the symbols. As far as the vertical discretisation is concerned, the wind $\mathbf{v}_k$, temperature T_k, specific humidity q_k, and linearised geopotential height G_k are defined at the full levels (k = 1,N); N is the total number of levels in the vertical. The pressure $p_{k+1/2}$, geopotential height $\Phi_{k+1/2}$, and vertical velocities $\dot{\eta}_{k+1/2}$ and $\dot{s}_{k+1/2}$ are defined at the 'half levels'. For the horizontal discretisation, the Arakawa C-grid is used for the grid point model and the Arakawa A-grid is used for the computations performed in grid point space in the spectral model.

The hybrid coordinate is defined in terms of the pressure as follows:

$$p_{k+1/2} = A_{k+1/2}(\eta) + B_{k+1/2}(\eta)p_s(\lambda,\theta) \tag{2.1}$$

where the choice of A and B defines the closeness of the system to the σ coordinates ($A = 0.$) or p coordinates ($B = 0.$).

The equations of motion can be expressed as follows in hybrid coordinates.

$$\frac{dT_k}{dt_k} = \left[\frac{\kappa T_v}{1+(\delta-1)q}\right]_k \left(\frac{\omega}{p}\right)_k + (P_T + K_T)_k, \tag{2.2}$$

$$\frac{d\mathbf{v}_k}{dt_k} = [-f\mathbf{k}\times\mathbf{v} - \nabla\Phi - R_d T_v \nabla lnp]_k + (\mathbf{P_u} + \mathbf{K_u})_k, \tag{2.3}$$

$$\Delta B_k \frac{d_H lnp_s}{dt_k} = -D_k \frac{\Delta p_k}{p_s} - (\dot{s}_{k+1/2} - \dot{s}_{k-1/2}), \tag{2.4}$$

$$\frac{dq_k}{dt_k} = (P_q + K_q)_k, \tag{2.5}$$

where q is the specific humidity.

$$\frac{d_H}{dt} = \frac{\partial}{\partial t} + \frac{u}{acos\theta}\frac{\partial}{\partial\lambda} + \frac{v}{a}\frac{\partial}{\partial\theta}, \tag{2.6}$$

and

$$\frac{d}{dt} = \frac{d_H}{dt} + \dot{\eta}\frac{\partial}{\partial \eta}; \tag{2.7}$$

In the temperature equation,

$$(T_v)_k = [1 + (\frac{1}{\epsilon} - 1)q_k]T_k, \tag{2.8}$$

and

$$\left(\frac{\omega}{p}\right)_k = \left(\frac{1}{p}\frac{dp}{dt}\right)_k. \tag{2.9}$$

In the momentum equations, for consistency, Φ and ∇lnp are defined at level k as

$$\Phi_k = \Phi_s + R_d \sum_{j=k+1}^{N} (T_v \Delta lnp)_j + R_d(\alpha T_v)_k, \tag{2.10}$$

where $\alpha_1 = ln2$ and $\alpha_k = 1 - (\Delta lnp/\Delta p)_k p_{k-1/2}$ for all other values of k;

$$(\nabla lnp)_k = \nabla\left(\frac{p_{k+1/2}\, lnp_{k+1/2} - p_{k-1/2}\, lnp_{k-1/2}}{\Delta p_k}\right). \tag{2.11}$$

In the mass equation the following short-hand notation has been used

$$\dot{s}_{k-1/2} = \frac{1}{p_s}\left(\dot{\eta}\frac{\partial p}{\partial \eta}\right)_{k-1/2}. \tag{2.12}$$

The terms $\mathbf{P_u}$, P_T and P_q represent the physical processes. The terms $\mathbf{K_u}$, K_T and K_q represent the contributions due to added horizontal diffusive processes.

For the grid point model the implementation of the semi-Lagrangian discretization of these equations has been described in MH2. For the spectral model, a full description is given in G95. The latter uses the same discretization as the former, except for the mass and temperature equations. For these, a two-time level version of the discretization described in Ritchie et al. (1994) is used.

Because they give different forecasts, as will be shown in the next section, we repeat here the two different methods of evaluating the vertical velocity used in MH2 and G95. In order to compute the departure point with an accuracy of $O(\Delta t^2)$ the vertical velocity is needed at time level $n + 1/2$. In MH2 this is accomplished as follows.

$$\dot{s}^{n+1/2} = (3\dot{s}^n - \dot{s}^{n-1})/2; \tag{2.13}$$

where $\dot{s}$ is updated every time step by substituting for $(lnp_s)^{n+1}$ and D^{n+1} in the following equation after the semi-implicit adjustment has been completed. We will call this a *prognostic* evaluation of of $\dot{s}$ in what follows.

$$B_{k+1/2}\,(lnp_s)^{n+1} + \left(\frac{\Delta t_+}{2}\right)\left\{\sum_{j=1}^{k}\frac{\Delta p_j^r}{p^r}\left[D_j^{n+1} - (N_p)_j^{n+1/2}\right] + (\dot{s})_{k+1/2}^{n+1}\right\} =$$

$$\sum_{j=1}^{k}\left\{\Delta B_j (lnp_s)_{*2,j}^{n} + \left(\frac{\Delta t_-}{2}\right)\frac{\Delta p_j^r}{p^r}\left[-D^n + (N_p)^{n+1/2} - \frac{p^r}{\Delta p^r}\Delta\dot{s}^n\right]_{*3,j}\right\}, \qquad (2.14)$$

On the other hand, in G95 the vertical velocity at time level $n + 1/2$ is computed *diagnostically* by first summing Eq. (2.4) over all levels to compute $(\partial lnp_s/\partial t)^{n+1/2}$ and subsequently summing partially to obtain $\dot{s}^{n+1/2}$:

$$(\dot{s})_{k+1/2}^{n+1/2} = -\left\{B_{k+1/2}\left(\frac{\partial lnp_s}{\partial t}\right) + \sum_{j=1}^{k}\left[\frac{\Delta p_j}{p_s}D_j^n + (\mathbf{v}_j.\nabla lnp_s)\Delta B_j\right]\right\}^{n+1/2}, \qquad (2.15)$$

The terms $v^{n+1/2}$, $p^{n+1/2}$, $(lnp_s)^{n+1/2}$ and $D^{n+1/2}$ are extrapolated as in Eq. (2.13).

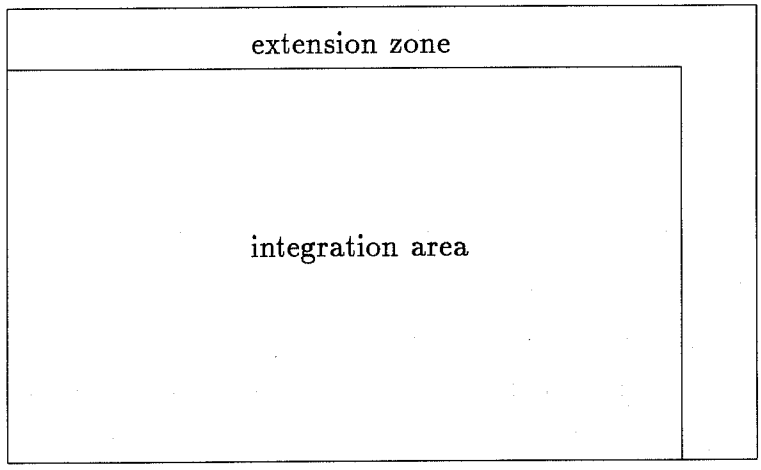

Figure 1. The area extension zone of the spectral model.

Because it enters into our debate in section 4 we briefly discuss here the 'bi-periodic problem' in the spectral model . The solution adopted is to extend the integration area. The geometry of the area extension zone is illustrated in fig. 1. It is important to stress that only data from the inner integration area are needed for its construction. This is first done immediately after the analysis and the first set of boundary fields are read

in. The extension zone is subsequently refreshed only when new boundary values are read in, that is, every six hours in the experiments described in the next section. All grid-point calculations (physics, non-linear dynamics, etc.) are carried out in the inner integration area only.

The extrapolation of gridpoint values to the extension zone is carried out in such a way that the subsequent Fourier transforms will give a smooth representation of the extended field in the inner area with preserved gradients normal to the lateral boundaries. The extrapolation is first carried out along each row of gridpoints in the x-direction and then along each column of grid point values in the y-direction. A sum of four trigonometric functions is utilized for each one-dimensional extrapolation. The required 4 coefficients are determined from the gridpoint values and from the gradients normal to the lateral boundaries. Since this extrapolation procedure is arbitrary a simple experiment to test the sensitivity to changes in the procedure is described below.

Another feature of the spectral formulation is the timing of the coupling to the applied boundary conditions. In the conventional approach, a boundary relaxation scheme (Davies, 1976) is applied at the end of each time step. This is how the boundary lines are updated in the gridpoint limited area model. For a spectral limited area model, such an application of the boundary relaxation would be expensive, however, since two extra Fourier transforms would be needed. To avoid this extra expense the boundary relaxation is performed immediately after all the other grid point computations have been completed, as suggested by Radnoti (1995). The result is that the semi-implicit 'u' equation now becomes

$$u(t+\Delta t)+(1+\epsilon_g)\Delta t\left(\frac{1}{\bar{h}_x}\frac{\partial}{\partial x}G(t+\Delta t)-\bar{f}v(t+\Delta t)\right)=(1-\alpha_B)A_u+$$

$$\alpha_B\left[u_B(t+\Delta t)+(1+\epsilon_g)\Delta t\left(\frac{1}{\bar{h}_x}\frac{\partial}{\partial x}G_B(t+\Delta t)-\bar{f}v_B(t+\Delta t)\right)\right] \qquad (2.16)$$

where ϵ_g denotes the semi-implicit 'de-centering' coefficient, A_u the right hand side of the semi-implicit 'u' equation as calculated in the inner integration area, $\bar{h}_x$ an area average of the mapfactor h_x, $\bar{f}$ an area average of the Coriolis parameter, α_B the boundary relaxation factor and u_B, v_B , G_B the lateral boundary condition fields.

Starting from area-extended and spectrally truncated initial fields in spectral space, the following sequence of calculations is carried out for each time-step of the spectral model:

(1) Inverse Fast Fourier transforms to obtain all horizontal derivatives and other quantities needed for the grid-point calculations are peformed.

(2) Grid-point calculations including non-linear dynamics, determination of trajectories, semi-Lagrangian interpolations, physics, and calculations of the right hand sides of the semi-implicit equations are done.

(3) Boundary relaxation of the right hand sides of the semi-implicit equations (see above) is carried out. The required boundary condition fields have been pre-calculated for e.g. every 6th hour and are linearly interpolated in time to each time-step.

(4) Direct Fast Fourier transform of the right hand sides of the semi-implicit equations are done.

(5) The semi-implicit equations are solved in spectral space.

(6) Implicit horizontal diffusion and time-filtering are carried out in spectral space.

For the forecasts described in the next section, a cosine-dependent boundary relaxation function was used (rather than the conventional tanh-dependent one), and there were 6 lines in the boundary relaxation zone. In discretizing in the vertical 16 hybrid levels were used. In the horizontal, 162×142 grid points were used for all forecasts, both on the 0.5° and 0.2° grids. For the spectral integrations, the transform grid consisted of the identical grid points. $T^r = 300°K$ and $p^r = 800hPa$. The fields at time level n+1/2 were estimated using the filtered two level extrapolation described by Eqs. (47) and (49) of MH2. One iteration of a trilinear interpolation is used in the trajectory calculation.

The physical paramaterization schemes are as described in Kållberg (1990). For a summary, see Gustafsson (1991). Both models use exactly the same physics.

3. COMPARISON OF FORECASTS.

In this section we show forecasts generated by both models, first on a 0.5° × 0.5° grid and subsequently on a 0.2° × 0.2° grid. We use the forecasts first to demonstrate some lessons we have learned about the spectral and grid-point models and secondly to compare and contrast their relative forecasting abilities.

For the tests on the $0.5° \times 0.5°$ grid we use the starting analysis of 0000 UTC 10 Jan. 1993. During the first 12h of the forecast period the already deep low at (55N,22W) in fig. 2 deepened by a further 46hPa to a record low value of 915hPa and moved to a position at (60N,15W). This rapid deepening provides a severe test for any model. We will use this data set to illustrate a lesson we learned about horizontal diffusion.

3a. Horizontal diffusion is needed to maintain stability in the lower atmosphere.

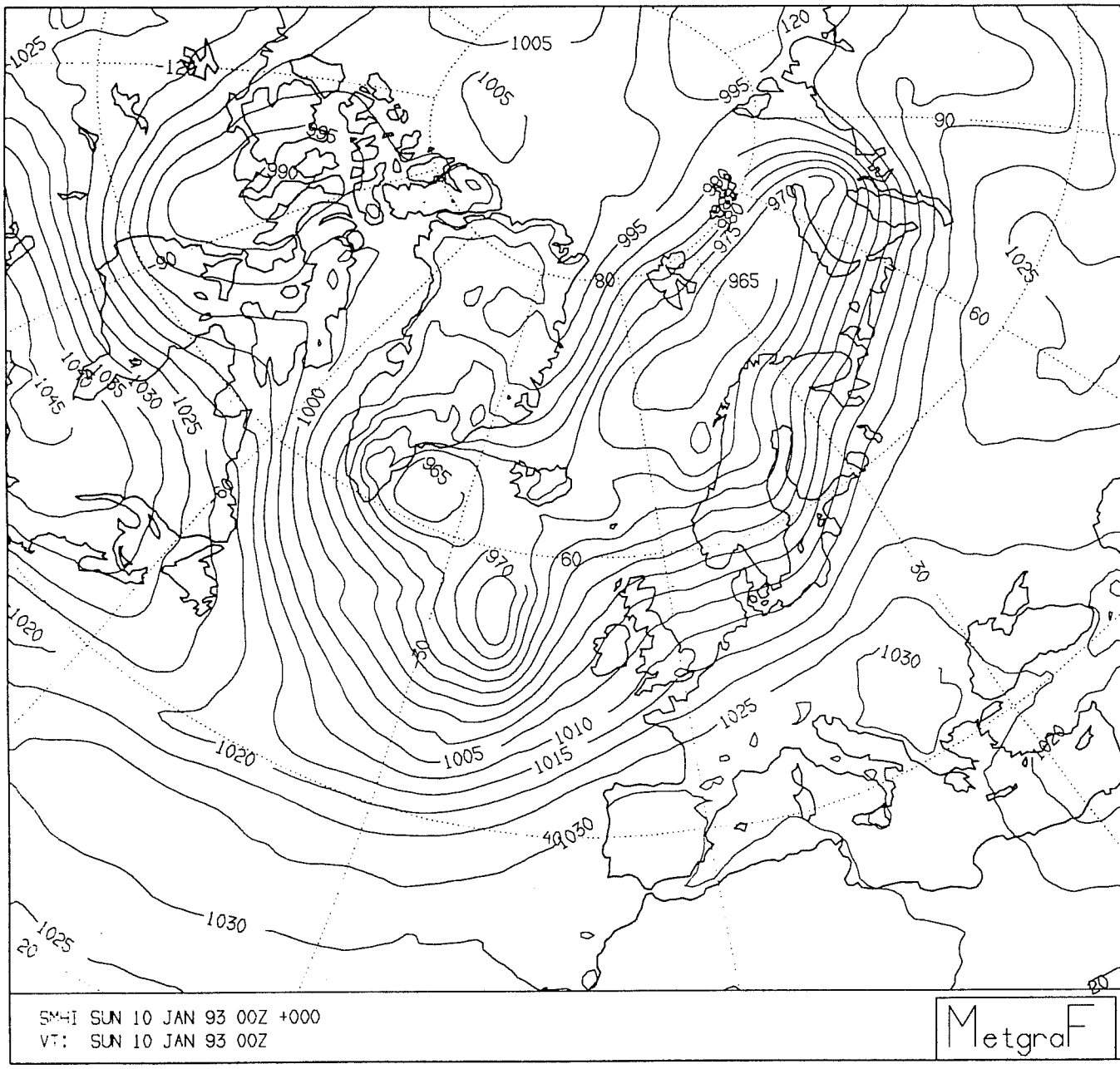

Fig. 2. The analysis of sea level pressure at 0000 UTC on 10 January, 1993.

Historically, in semi-Lagrangian integrations, it was not found necessary to use horizontal diffusion. This was demonstrated on a relatively coarse grid with simple physics by McDonald (1985), and also on a $0.5° \times 0.5°$ grid with sophisticated physics for a reasonably active data set; see MH2. It was hoped that this would hold in general for the following reason. If it is necessary to apply horizontal diffusion with a large time step, as is typically the case in semi-Lagrangian integrations, then an implicit scheme must be used in order to maintain stability. In a grid point model this is computationally expensive. The 'world record storm' integration destroyed that hope. During the rapid deepening an instability developed in the lower atmosphere near the deep low in the grid-point forecast.

The tests described in MH2 had indicated that the following choice of damping coefficients should have provided sufficient damping of gravity wave noise to give stable forecasts with a time step of 20 minutes: for the 'de-centering' coefficient, $\epsilon_g = 0.1$; and for the coefficient of the filter for the non-linear terms, $\epsilon_N = 0.1$. This proved not to be the case for 'world record storm' data set. The 12h forecast of 2 metre temperature produced by the grid-point model is shown in fig. 3. Severe noise has developed in the vicinity of the deep low. Increasing ϵ_g and ϵ_N did not eliminate this noise. The forecast produced by the spectral model which uses the same time step, the same choice of ϵ_g and ϵ_N, but with implicit horizontal diffusion added ($K = 2.5 \times 10^{14}$) is shown in fig. 4. The severe noise is absent. Repeating the spectral integration without horizontal diffusion and with a spectral truncation at waves corresponding to 2 grid-lengths yields a forecast with the same noise as the grid-point integration. We must conclude that horizontal diffusion is needed in the latter. See fig. 5, which again shows the 12h forecast of 2 metre temperature produced by the grid point model but now using implicit fourth order diffusion of u, v, T and q with a coefficient of $K = 5 \times 10^{14}$; (see discussion below). As can be seen, this forecast is now noise-free and agrees well with the spectral forecast.

In the grid point model the fourth order diffusion scheme solves the equation

$$\frac{\partial f}{\partial t} + K\left(\frac{\partial^4 f}{\partial x^4} + \frac{\partial^4 f}{\partial y^4}\right) = 0, \tag{3.1}$$

whereas in the spectral model the fourth order diffusion scheme solves the equation

$$\frac{\partial f}{\partial t} + K\left(\frac{\partial^4 f}{\partial x^4} + 2\frac{\partial^4 f}{\partial x^2 \partial y^2} + \frac{\partial^4 f}{\partial y^4}\right) = 0. \tag{3.2}$$

Obviously, a larger value of K is required in Eq. (3.1) than in Eq. (3.2) to give the same amount of diffusion.

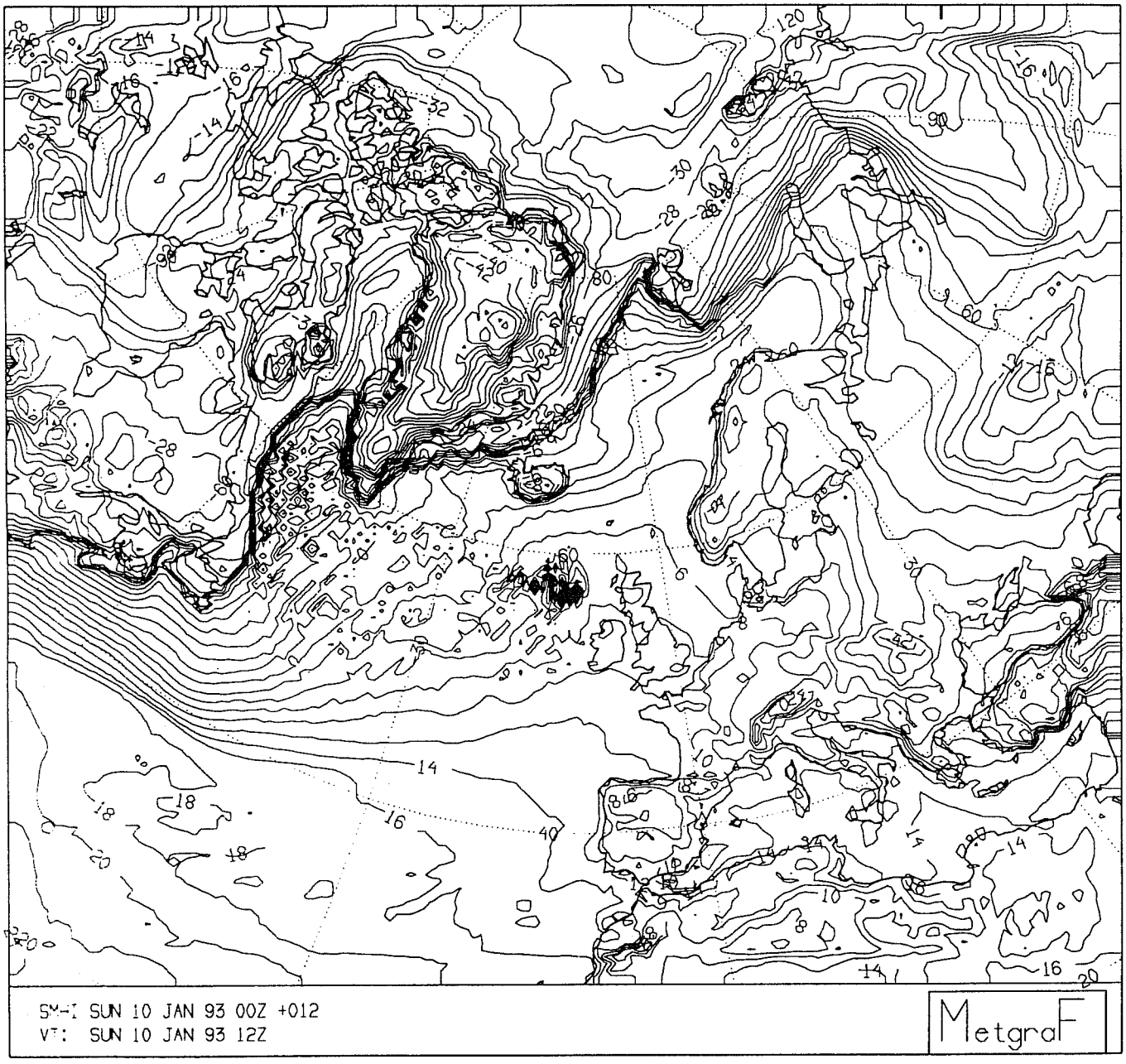

Fig. 3. The 12h forecast of 2 metre temperature starting from the analysis of 0000 UTC 10 January, 1993 using $\epsilon_g = 0.1$ and $\epsilon_N = 0.1$ and no horizontal diffusion. This forecast was generated by the grid point model.

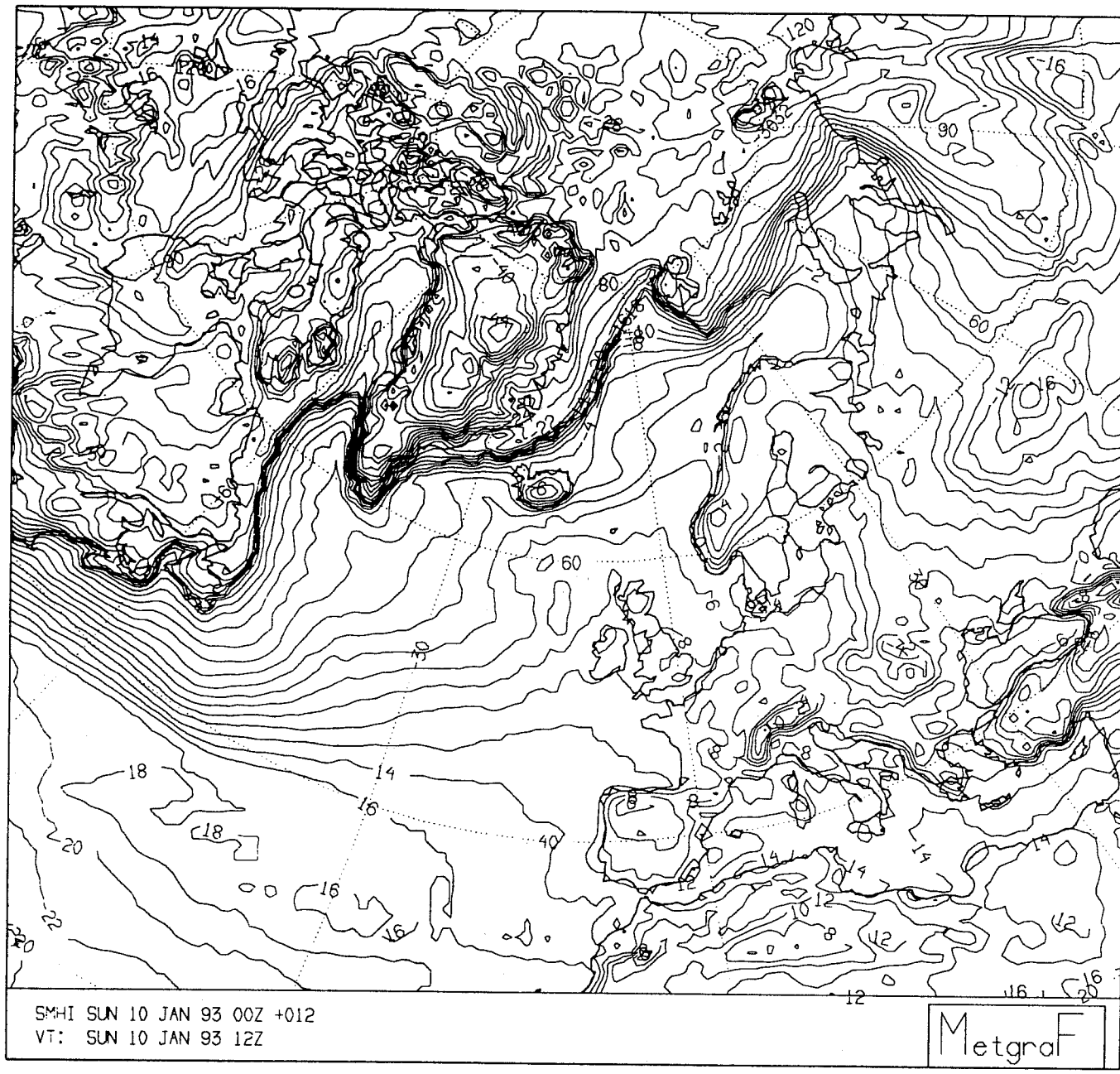

Fig. 4. Same as fig. 3, except that the spectral model was used with a 3 grid length wave truncation and implicit horizontal diffusion was applied with a coefficient of $K = 2.5 \times 10^{14}$.

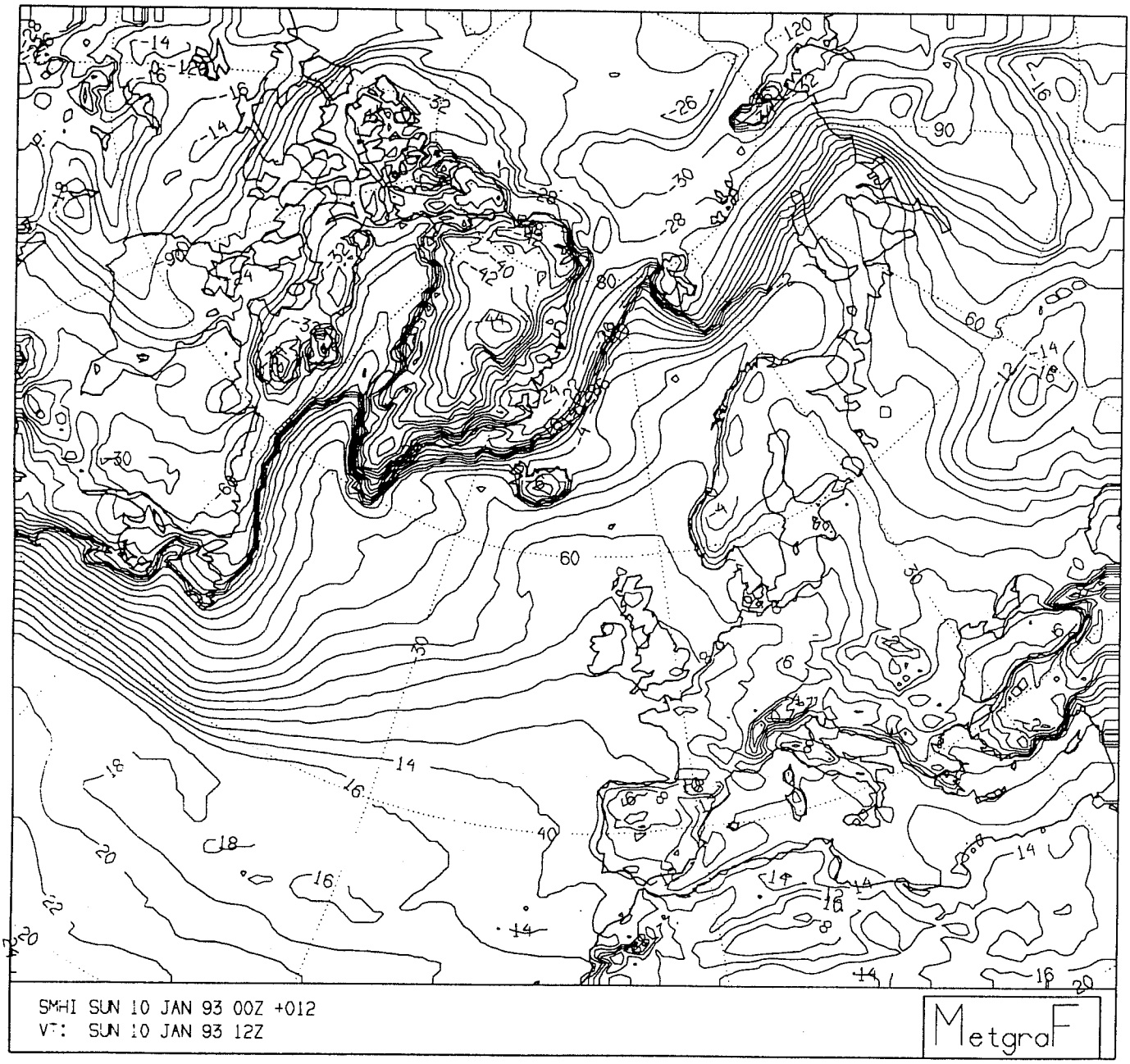

Fig. 5. Same as fig. 3, except that fourth order horizontal diffusion of u, v, T, and q has been applied with a coefficient of $K = 5 \times 10^{14}$.

Although Eq. (3.2) might be considered more desirable, Eq. (3.1) was used in the grid point model simply because it was so much easier to solve in a computationally efficient manner. This points to an advantage of the spectral over the grid-point approach. Unwanted noise is generated in numerical weather prediction models, by the orography, by the boundaries, by the 'physics', or even sometimes by the dynamics. The spectral approach provides two useful filters for attacking this problem *at no computational cost.* Two grid noise can be eliminated simply by changing a parameter. Also implicit diffusion of any order can be programmed very simply with, for instance, sixth order being no more expensive than fourth order diffusion, both being 'free'. Contrast this with the grid-point model where any of these filters have finite computational costs. We shall return to this point in section 4.

3b. The spectral model is insensitive to the area extension formulation

The technique of extending initial and lateral boundary fields to obtain bi-periodic variations in both horizontal directions was briefly described in section 2. The extrapolation is carried out in a such a way that the field itself and the gradients of the field normal to the boundary are preserved along the boundaries of the inner integration area. In order to test the sensitivity of the spectral forecasts to the formulation of this area extension, a forecast experiment, with the requirement on preserved normal gradients excluded, was carried out. All other aspects of the spectral model integrations were identical. The result of this sensitivity experiment is illustrated by the difference field between +12 h pressure forecasts valid at 12UTC 10 January 1993 in fig. 6. There are only pressure differences of the order of a few tenths of a hPa, and we may conclude that the spectral model is rather insensitive to details in the formulation of the area extension to obtain bi-periodic variations.

For the tests on the $0.2° \times 0.2°$ grid we use the starting analysis of 0000 UTC 11 Jan. 1987. The meteorological phenomenon occurring on this date is the formation of convective snow-bands over the Baltic Sea when there is a persistent cold easterly airflow over northern Europe. For a detailed discussion see Andersson and Gustafsson (1994). We felt that the following questions could be addressed by looking at forecasts starting from such a data set. Can the semi-Lagrangian schemes forecast the sharp bands of precipitation seen over the Baltic Sea and other fine details caught by the Eulerian model using the same grid? If so, will the spectral model have problems describing such sharp bands? We examine these issues in what follows.

Again, for the grid point model integrations, the horizontal grid consisted of $162 \times$

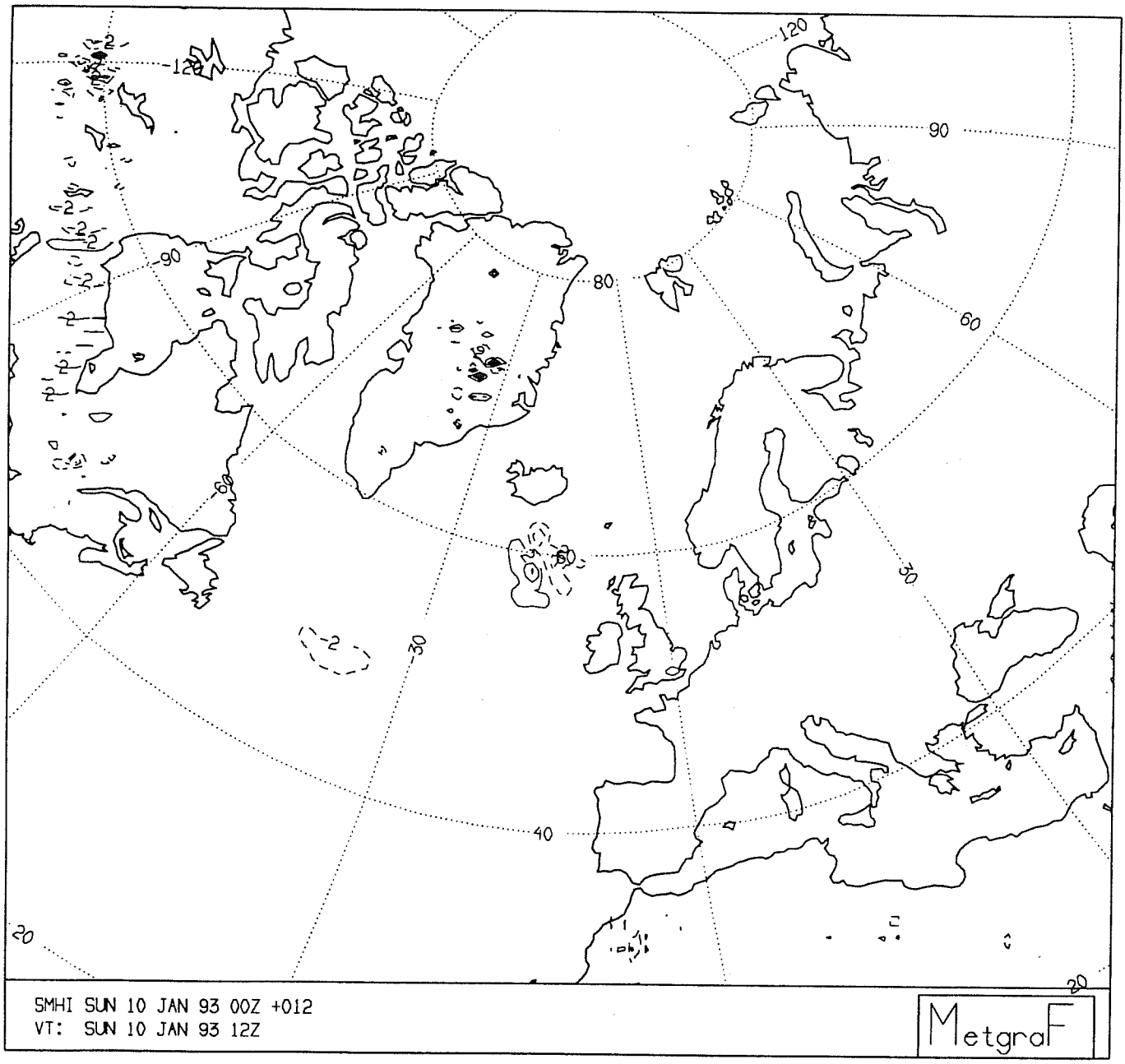

Fig. 6. Difference between mean sea level pressure forecasts at 0000 UTC, 10 January, 1993 + 12h produced by the spectral model with different algorithms for the area extension. The isolines are every 0.2 hPa.

142 grid points with a spacing of $0.2^\circ \times 0.2^\circ$ and exactly the same horizontal grid was used for the spectral model transform grid. Otherwise the models were as described in section 2.

3c. The vertical velocity at time level $n + 1/2$ should be computed *diagnostically.*

There are two schools of thought on how to compute the vertical velocity, the *prognostic* school, who advocate Eq. (2.14) and the *diagnostic* school, who advocate Eq. (2.15). We had not seen any clear evidence to prefer one over the other during our experiments on the $0.5^\circ \times 0.5^\circ$ grid. However, on the $0.2^\circ \times 0.2^\circ$ grid, we see a notable difference in the sensible heat flux chart. The *prognostic* computation the vertical velocity at time level $n + 1/2$ yielded the noisy 18 hour forecast shown in fig. 7. Its *diagnostic* computation, on the other hand, yielded the noise-free forecast shown in fig. 8. This noise can also be seen in the divergence field at the lowest model levels, but not in the upper atmosphere. The remaining forecasts shown in this section will always use Eq. (2.15) to evaluate the vertical velocity at time level $n + 1/2$.

3d. The semi-Lagrangian grid point model maintains the sharpness of the convective fronts.

The convective snow-bands we wish to concentrate on can be clearly seen in the satellite image, see fig. 9. The Eulerian model using a 2 min. time step and $K = 0.5 \times 10^{13}$ for the fourth order explicit diffusion scheme does a good job of modelling these bands. See fig. 10, which shows the 18h - 6h accumulated precipitation forecast.

With a time step of 6 minutes the grid-point semi-Lagrangian scheme gives a very similar forecast. See fig 11, which again shows the 18h - 6h accumulated precipitation forecast. Notice that the convective band seems to have sharpened slightly over the East coast of Sweden. For this forecast we used 4th order implicit diffusion with $K = 6.0 \times 10^{11}$. It is possible to obtain a stable forecast with a time step of 7.5 minutes also. See fig. 12, which again shows the 18h - 6h accumulated precipitation forecast.

3e. The semi-Lagrangian spectral model gives forecasts in good agreement with those produced by the Eulerian grid point model.

Forecasts produced by the spectral semi-Lagrangian model using the same time step (7.5 min.), ϵ_g , ϵ_N and effective diffusion ($K = 3.0 \times 10^{11}$) as the grid point semi-Lagrangian model agree very well with the Eulerian grid point model. See fig. 13, and

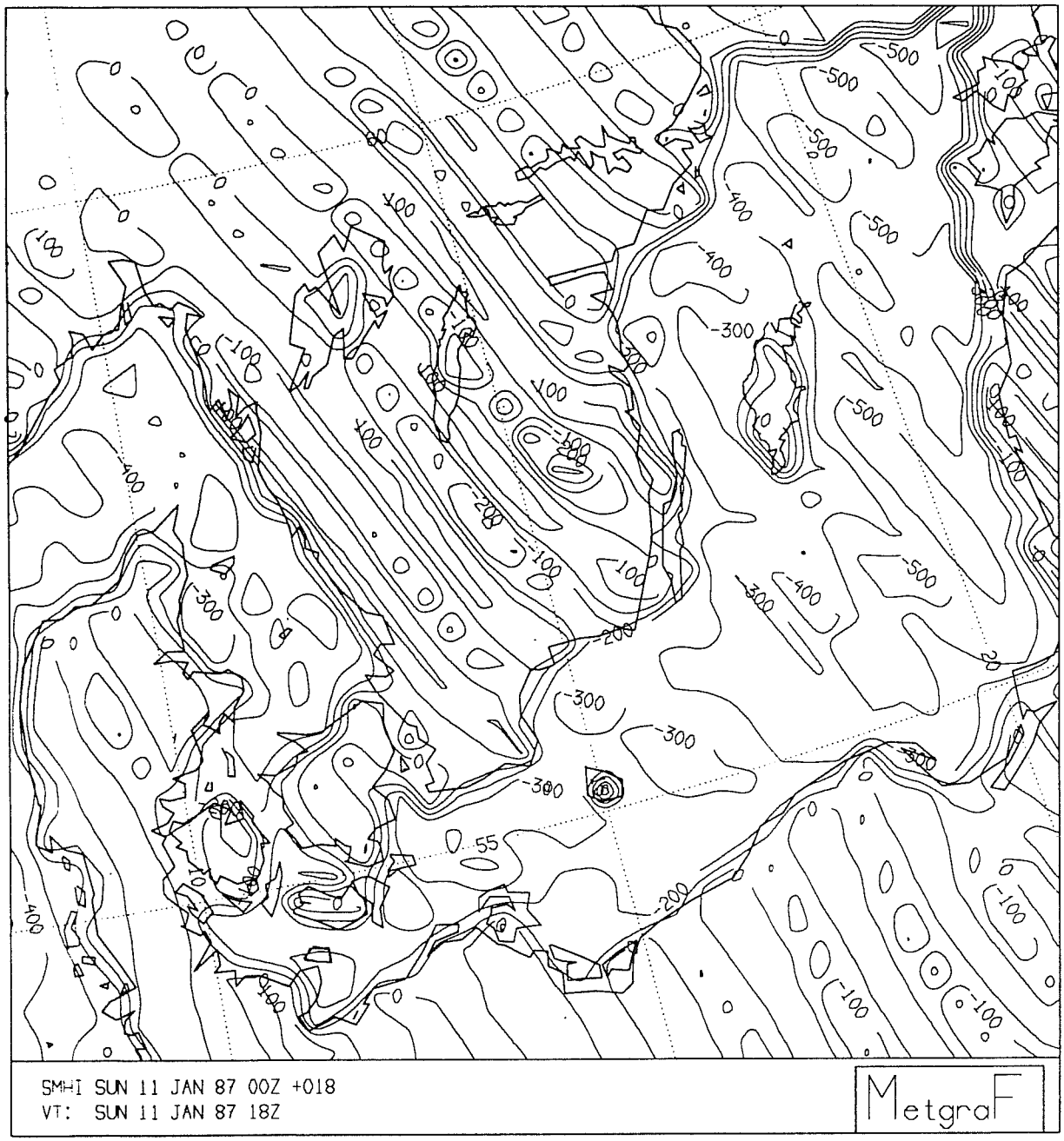

Fig. 7. The 18h forecast of sensible heat flux starting from the analysis of 0000 UTC 11 January, 1987 using the *prognostic* computation of $\dot{s}$. The area shown includes Denmark, southern Sweden, and the Baltic sea.

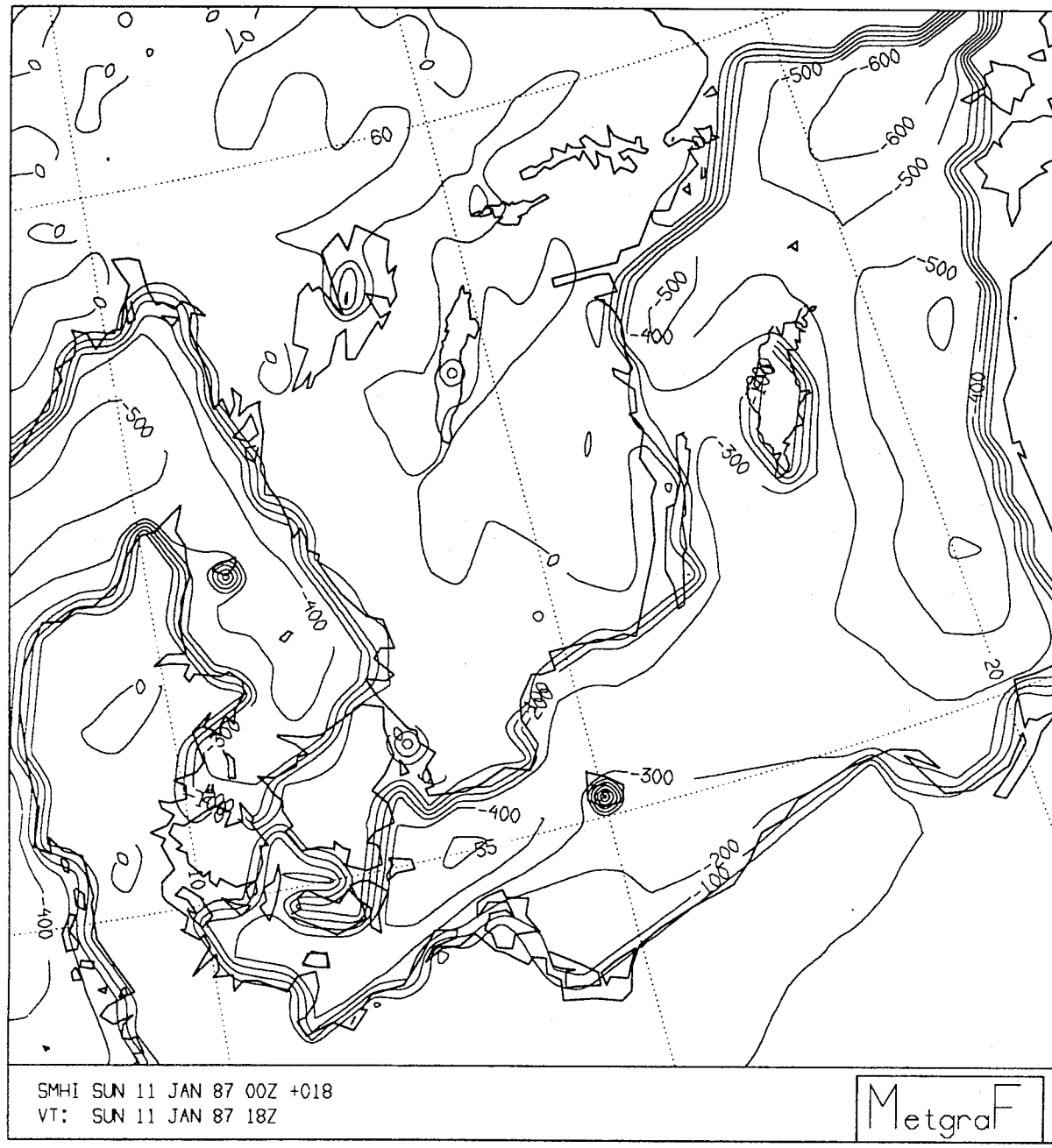

Fig. 8. Same as fig.7, except that the *diagnostic* computation of $\dot{s}$ was used.

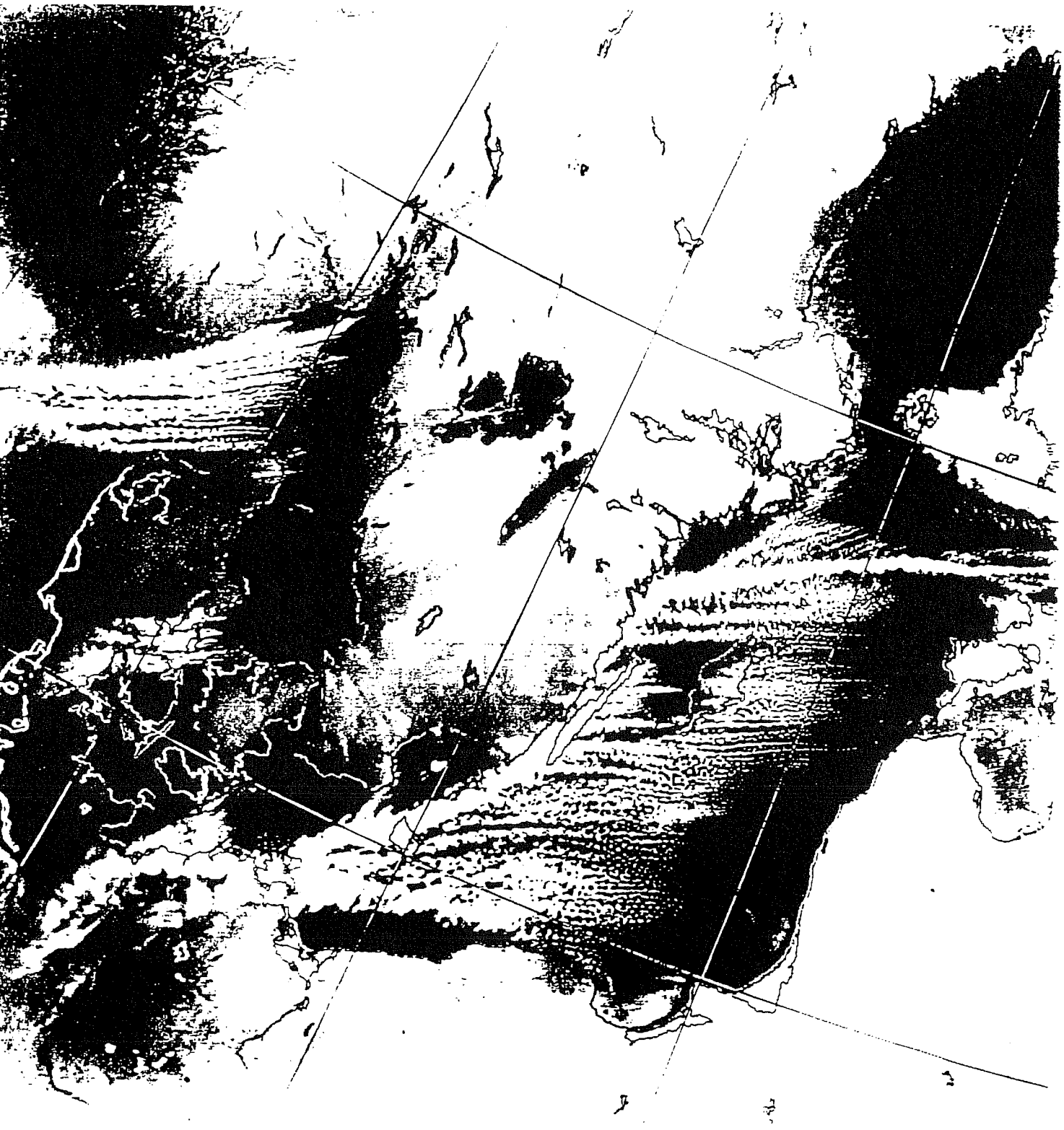

Fig. 9. NOAA infra-red satellite image valid at 1235 UTC 11 January, 1987.

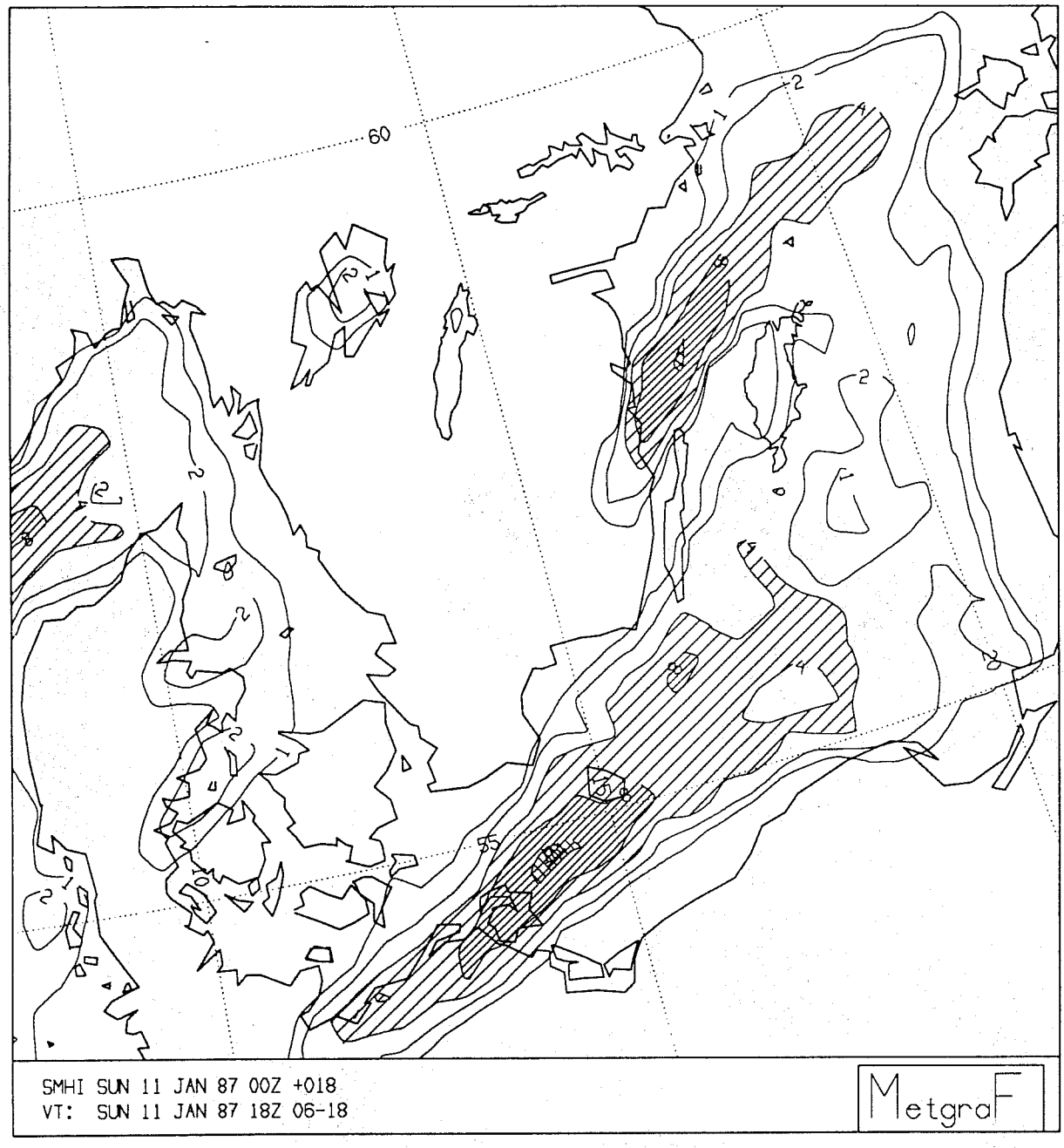

Fig. 10. The 1800 - 0600 accumulated precipitation forecast for 11 January, 1987, produced by the Eulerian model using a 2 min. time step. Fourth order explicit diffusion was applied with $K = 0.5 \times 10^{13}$.

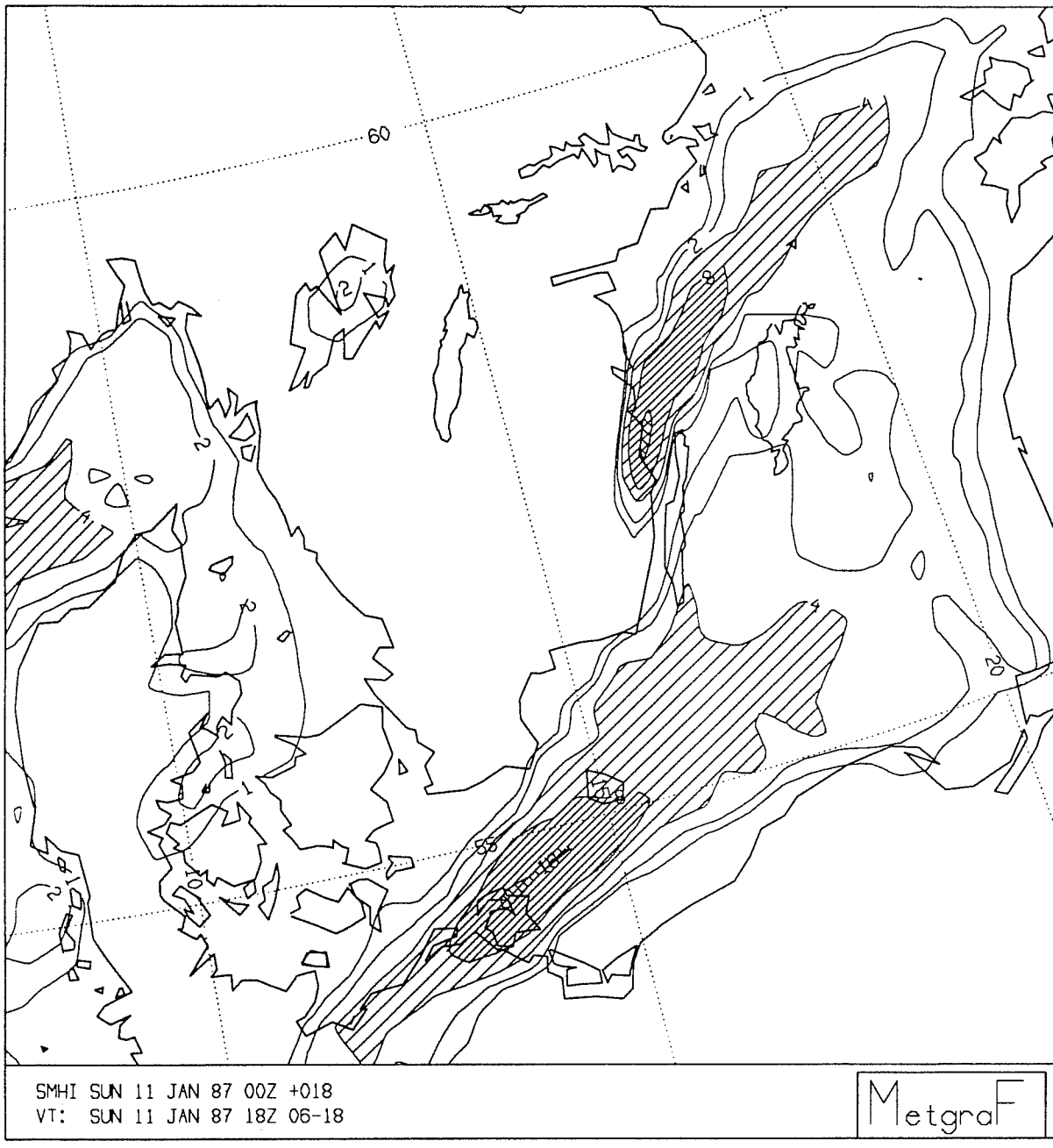

Fig. 11. The 1800 - 0600 accumulated precipitation forecast for 11 January, 1987, produced by the semi-Lagrangian model using a 6 min. time step. Fourth order implicit diffusion was applied with $K = 6.0 \times 10^{11}$.

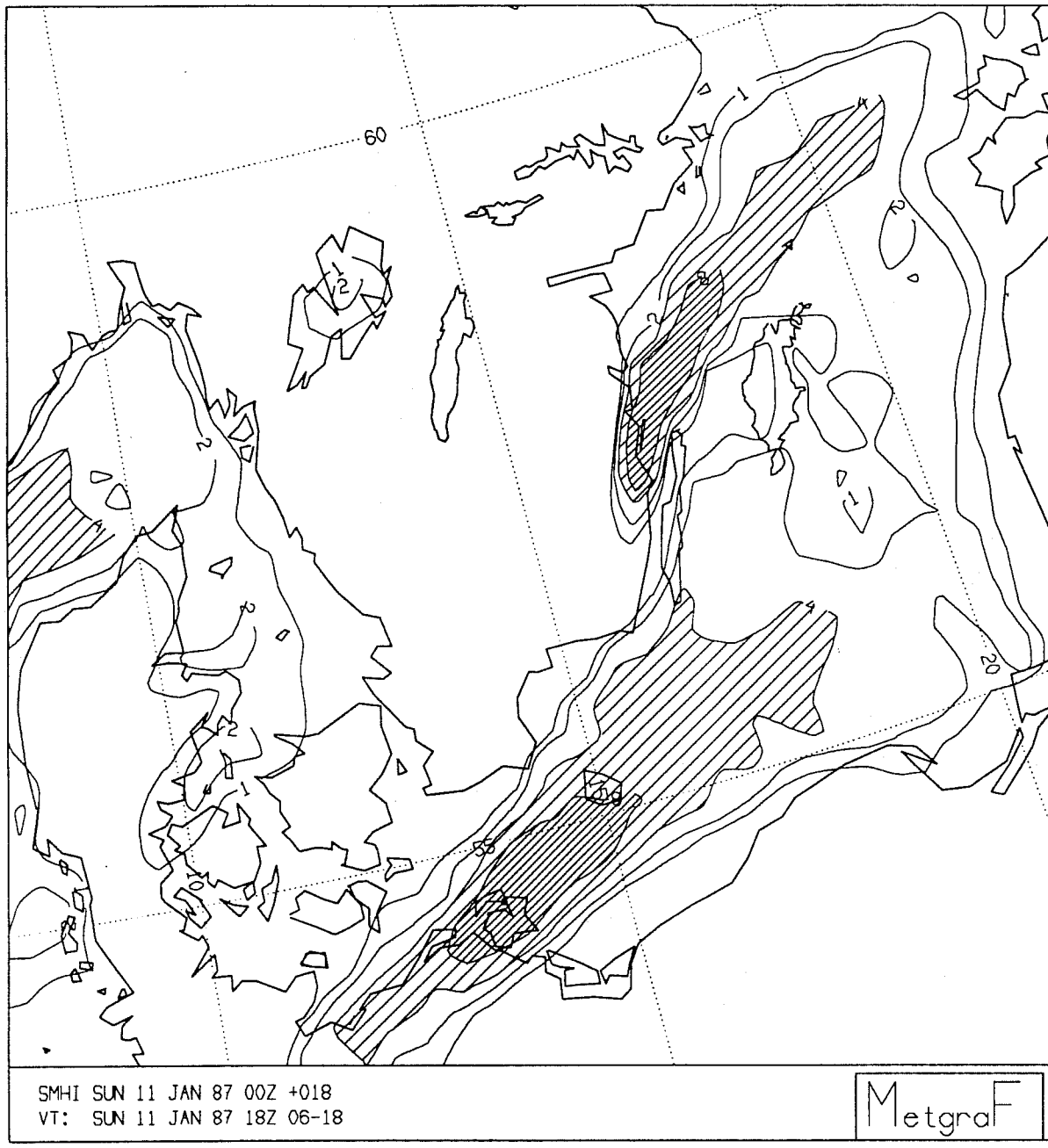

Fig. 12. Same as Fig. 11, but with a time step of 7.5 minutes.

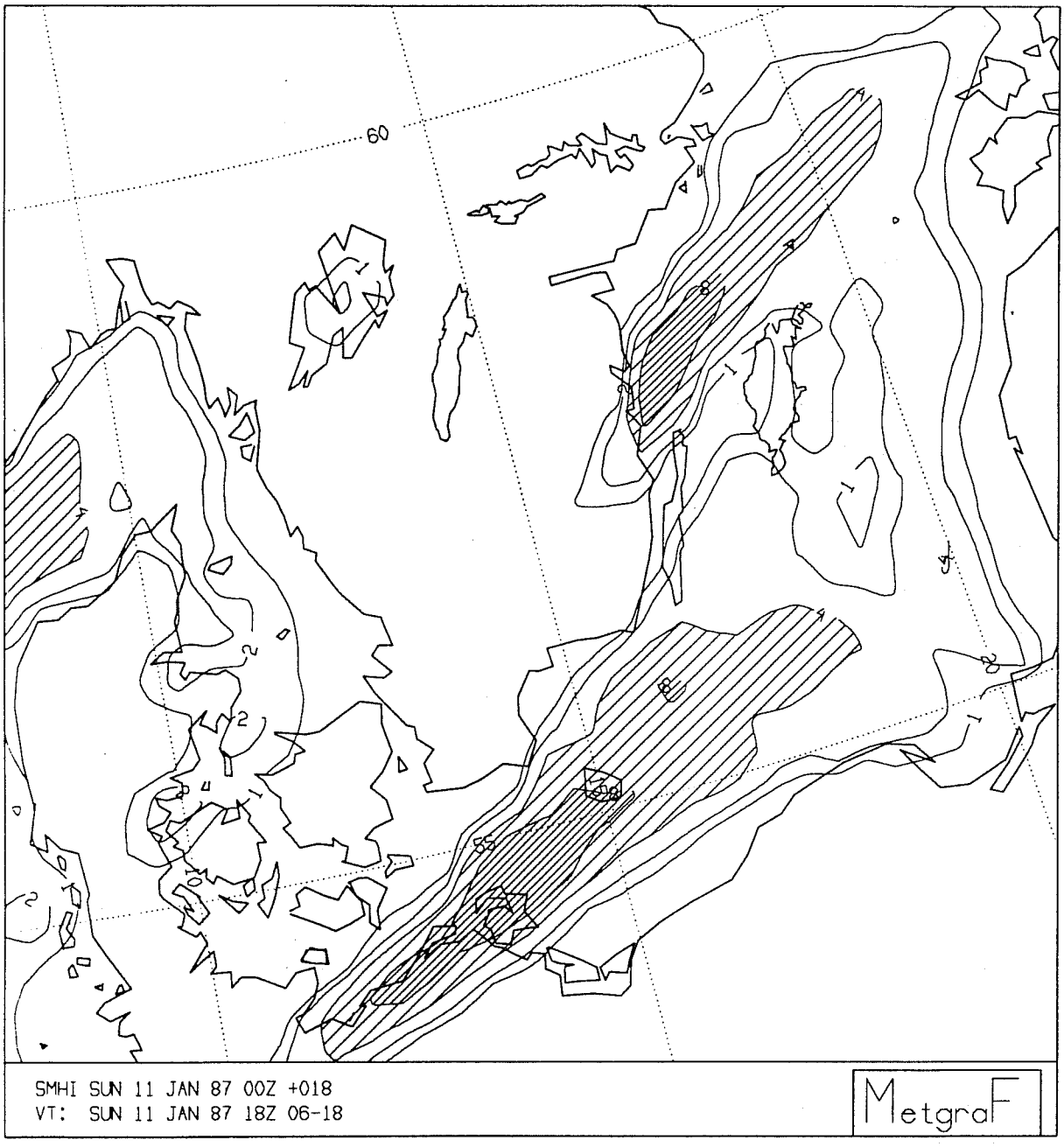

Fig. 13. Same as Fig. 12, but produced by the spectral semi-Lagrangian model with a wave truncation of 3 grid lengths and with implicit horizontal diffusion applied with a coefficient of $K = 3 \times 10^{11}$.

compare it with fig. 10. The increased sharpness seen in the grid-point Semi-Lagrangian forecast is absent, however.

The standard three grid length wave truncation was applied in this spectral semi-Lagrangian model integration. This truncation is normally used in spectral models in order to avoid aliasing of quadratic terms during calculations on the transform grid when an Eulerian time integration scheme is used. In contrast, the semi-Lagrangian time integration scheme treats the advection terms, the main source of this problem, in an alias-free fashion. As a result, the three grid length wave truncation is no longer needed, and one is free to shift the level of spectral cut-off towards shorter wave lengths, while maintaining the same spectral transform grid.

We repeated the forecast of the convective snow-bands, but with a spectral wave-length cut-off at 2 grid lengths instead of 3. The outcome is shown in fig. 14. The convective snow-bands have sharpened slightly over the East coast of Sweden. It is not clear why the grid point semi-Lagrangian model predicts sharper snow bands over the east coast of Sweden than the spectral model run in this mode.

4. DISCUSSION

4a. The computer costs.

For the two test cases discussed above, we have shown that the spectral and the gridpoint semi-Lagrangian limited area models give approximately the same forecast accuracy. For the selection of which model to apply for operational weather forecasting, computer economy is a relevant criterion. The CPU timings in seconds on a CONVEX C-3840 vector computer for one time-step with both versions of the semi-Lagrangian HIRLAM model are contained in columns 2 and 3 of Table 1. As can be seen, the total CPU-time per timestep of the two models is approximately the same; the differences are within the accuracy of the timing measurements. The fraction of the total time spent in Fourier transforms for the spectral model is approximately 20 %. It is interesting to note that this extra time used by the spectral model is almost equal to the additional time spent by the grid point model in the semi-implicit solver, the implicit horizontal diffusion scheme, the calculation of finite difference operators in the non-linear dynamics, the de-staggering and staggering needed for the physics, and computing the coefficients needed to do the semi-Lagrangian interpolations for the u, v, and T points separately on the C-grid.

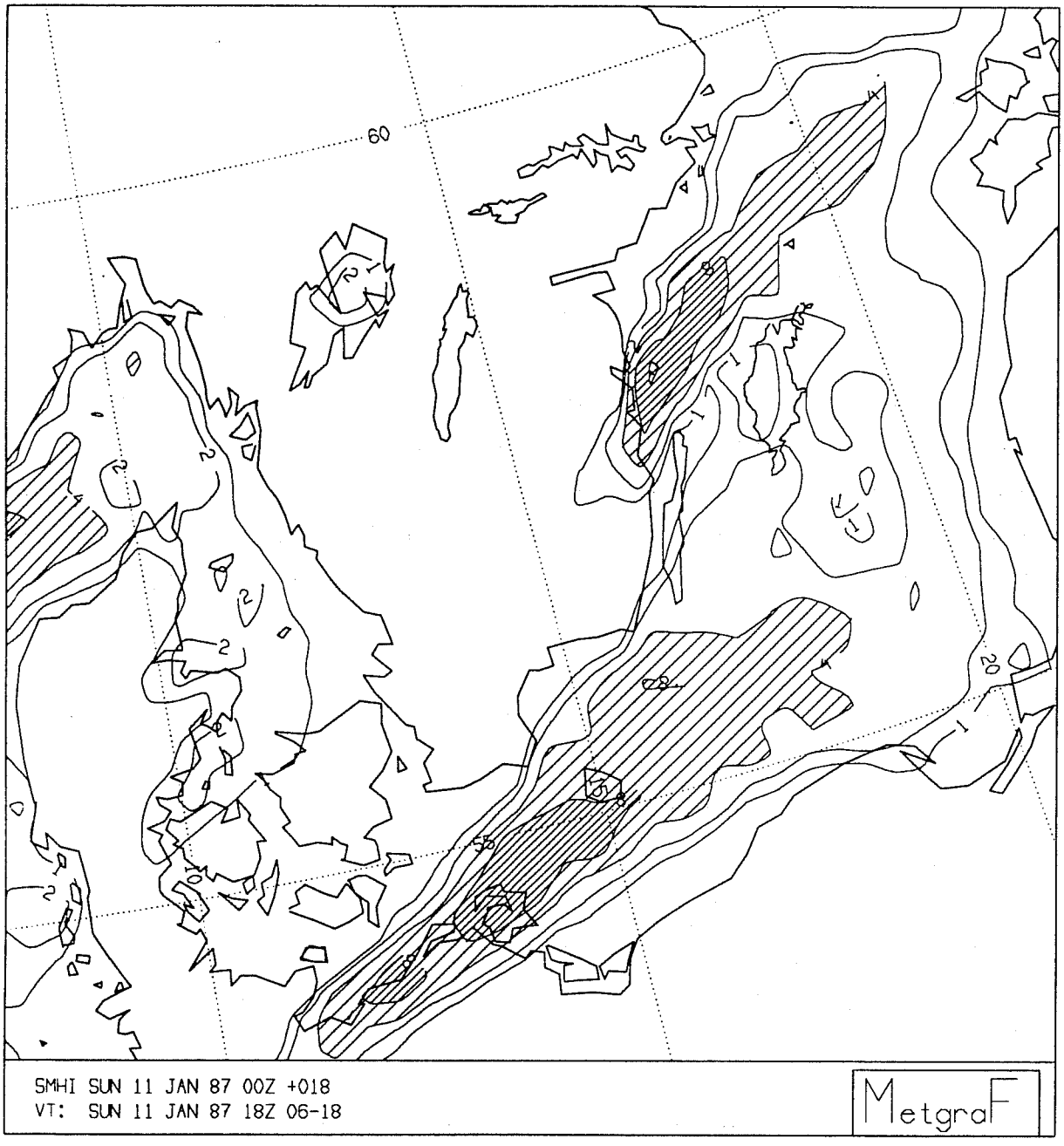

Fig. 14. Same as Fig. 13, but with a wave truncation of 2 grid lengths.

COMPUTATION	SPEC(CVX)	GRID(CVX)	GRID(CRAY)	GRID(SGI)
Fourier transforms	4.2 (21%)			
Non-linear dynamics	1.0 (5%)	1.2 (6%)	(5%)	(8%)
Semi-Lagrangian	7.3 (37%)	7.6 (38%)	(27%)	(29%)
Physics	6.5 (33%)	6.6 (33%)	(51%)	(48%)
Semi-implicit part	0.5 (3%)	1.8 (9%)	(6%)	(7%)
Implicit hor. diff.	0.1 (1%)	2.7 (13%)	(10%)	(8%)
Boundary relaxation	0.2 (1%)	0.2 (1%)	(1%)	(1%)
Total per time-step	19.8(101%)	20.2(100%)	(100%)	(101%)

Table 1 : The CPU-time in seconds, measured on a single processor CONVEX C-3810 computer, for the various types of calculations during one time-step of the spectral model (in column 2) and of the grid-point model (in column 3). In column 4 is listed the % CPU for the grid-point model measured on a single processor CRAY . In column 5 is listed the % CPU for the grid-point model measured on a single processor SGI Challenge.

It is worth pointing out, however, that these numbers are somewhat machine dependent. The identical code, which is fully vectorised, run on another vector machine, a CRAY, tells a slightly different story. See column 4 of table 1. During the the grid-point integration, the percentage of time spent in doing the semi-implicit adjustment and implicit horizontal diffusion is less than on the CONVEX computer. A similar message emerges from column 5, which gives the percentage times for a scalar machine, the SGI Challenge. The implicit diffusion code has been somewhat optimised for the scalar machine in the latter case. All other code is identical.

4b. **The relative advantages of the spectral and grid-point methods.**

The advantages and disadvantages of the spectral discretization relative to the grid-point discretization have been discussed in the literature. See, for instance, Gordon and Stern (1982) and Jarraud and Simmons (1983). It is interesting to review them and to see whether developments since that date, and in particular the implementation of the semi-Lagrangian schemes, causes us to re-appraise our opinions. Below we list the main advantages and disadvantages claimed for the spectral method and comment on them where we think the semi-Lagrangian schemes, or other advances, have made a difference.

Advantages of the spectral method.

1. It has no linear phase error. This was regarded as probably the most important advantage of the spectral over the grid-point method by Jarraud and Girard (1983), an opinion formed as a result of an extensive quasi-operational comparison. *Comment.* If the advection term is computed using the semi-Lagrangian approach then the linear phase error will be the same in the spectral and grid point integrations.

2. It has no 'coupling errors'. These originate from the inexact computation of horizontal non-linear differential operators. As an example, Jarraud and Simmons (1983) compute the horizontal Jacobian in spectral and grid point space and they demonstrate that the latter computation is such as to 'understimate the interactions between the various scales, and in particular the shortest scales, and to act as an effective reduction of the resolution'. Again, Jarraud and Girard (1983), as a result of their quasi-operational comparison confirmed this effective coarsening of the resolution. *Comment.* This advantage seems unaffected by the introduction of semi-Lagrangian differencing.

3. It has no pole problem for spherical harmonics with triangular truncation. *Comment.* Using the semi-Lagrangian approach enables one to overcome this difficulty in the grid-point model.

4. It has no aliasing problem for computation of quadratic terms. *Comment.* Using the semi-Lagrangian approach removes this difficulty from the grid-point model.

5. The Helmholtz equation generated by the semi-implicit time differencing scheme can be solved trivially. *Comment.* This advantage is reduced in importance once a 'fast solver' has been constructed for the grid point scheme.

6. Implicit horizontal diffusion is 'free' and almost infinitely tunable. For instance, high order diffusion can be used at no extra expense. Also, different diffusion coefficients can be used for different wave numbers. *Comment.* In the grid-point approach sophisticated diffusion schemes can be constructed. However, they are usually computationally expensive.

7. Spectral truncation provides another powerful 'free' method of controlling noise in the integration. *Comment.* It is possible to mimic these effects in a grid point model, by using Raymond or Shapiro filters for instance, but at some computational expence.

8. A motivation for the development of the HIRLAM spectral model was for the potential utilization in 4-dimensional variational data assimilation. The spectral technique offers an advantage since Fourier transforms are self-adjoint and this simplifies the development of the adjoint models that are needed for 4-dimensional data assimilation.

It is an additional advantage that it is rather straightforward to apply variational data assimilation with the incremental approach, i.e. a spectral model can easily be integrated with different resolutions during different iterations of the minimization process just by changing the spectral truncation.

9. The spectral model uses the Arakawa A-grid. Grid-point models are often written on the Arakawa C-grid. As a result, extra computations are needed on the latter whenever quantities defined at 'wind-points' are needed at 'temperature-points' and vice versa.

10. The combination of the spectral method with the reduced Gaussian grid (Hortal and Simmons, 1991) provides a neat solution to the problem of defining an almost uniform resolution over a sphere.

Disadvantages of the spectral method.

1. It may resolve sharp features (fronts, orography) less well than grid point models.

2. The truncated spectral representation of water vapour is not positive definite and a more elaborate negative borrowing scheme is required. *Comment.* Integrating the water vapour equation with a 'shape preserving' semi-Lagrangian scheme in grid point space within the spectral model overcomes this objection.

3. Spurious orographic and physical effects may result from Gibbs oscillations, with, for instance, 'negative mountains' occurring at the edges of land masses. *Comment.* Variational techniques for minimizing these spectral ripples over e.g. sea and coastal areas have recently been applied successfully, see Bouteloup (1995).

4. For limited area models the non-periodicity of the boundaries causes problems for which there is no unique solution. *Comment.* It was demonstrated above that this problem is a minor one.

5. Post-processed geopotentials and sea level pressure fields from the HIRLAM spectral model have been associated with small scale noise due to the non-linear coupling between surface pressure, orography and model level temperature. *Comment.* This problem was solved by Gustafsson (1995) by introduction of an iterative technique during truncation of surface pressure.

6. It has been shown to be advantageous to apply horizontally varying horizontal diffusion coefficients in the HIRLAM gridpoint model, e.g. to apply less horizontal diffusion of moisture along coastlines (Jens Hesselbjerg, Danish Meteorological Institute, personal communication). *Comment.* This form of diffusion is no longer free of computational cost in the spectral model.

5. CONCLUDING REMARKS

We have investigated the forecasting of two extreme atmospheric phenomena by a semi-Lagangian limited area model in its gridpoint as well as in its spectral formulation. The first case was the "World Record Low" of Janunary the 10th 1993, which was studied using a grid resolution of 55 km. The second case, which was studied with a grid resolution of 22 km, included intensive convective snowbands over the Baltic Sea during the cold winter of 1987. With minor variations, both models now produce very similar forecasts for the two extreme cases studied and the computer costs for the two model formulations are almost the same.

We have discussed advantages and disadvantages of the spectral versus the gridpoint technique for limited area modelling. This discussion seems to point toward an ideal model which is a composite of the two approaches consisting of a grid-point treatment of the 'physics', the non-linear terms, the specific humidity and cloud water mixing ratio equations, as well as all of the advection terms, combined with a spectral treatment of linear derivatives, the Helmholtz equation and horizontal diffusion.

Acknowledgements. We thank Jan Erik Haugen for supplying the CPU timings on the CRAY computer used in table 1, and Peter Lynch for his constructive criticism of the manuscript.

APPENDIX

List of variables and constants.

a	Radius of the earth (6.371×10^6 m)
c_{pd}	Specific heat of dry air (1004.64 J $kg^{-1}K^{-1}$)
c_{pv}	Specific heat of moist air (1869.46 J $kg^{-1}K^{-1}$)
δ	c_{pv}/c_{pd}
ϵ	R_d/R_v
ϵ_g	De-centered damping coefficient
ϵ_N	Filter coefficient
η	Vertical coordinate
$\dot{\eta}$	η -vertical velocity
$f = 2\Omega sin\theta$	Coriolis parameter (s^{-1})
g	Acceleration due to gravity (9.80665 m s^{-2})
κ	R_d/c_{pd}

K	Horizontal diffusion coefficient
λ	Longitude
N	Number of vertical levels
Ω	Angular speed of the earth (7.292×10^{-5} s^{-1})
p	Pressure (Pa)
p^r	Reference pressure for semi-implicit scheme (Pa)
p_s	Surface pressure (Pa)
Φ	Geopotential (g $\times$ height) (m^2 s^{-2})
Φ_s	Surface geopotential (m^2 s^{-2})
q	Specific humidity (kg kg^{-1})
R_d	Gas constant for dry air (287.04 J kg^{-1} K^{-1})
R_v	Gas constant for water vapour (451.51 J kg^{-1} K^{-1}
$\dot{s}$	Vertical velocity
t	Time (s)
T	Temperature (K)
T^r	Constant temperature for semi-implicit scheme(K)
T_v	Virtual temperature (K)
θ	Latitude
u	Zonal velocity (m s^{-1})
v	Meridional velocity (m s^{-1})

REFERENCES.

Andersson, Tage, and Nils Gustafsson 1994: Coast of departure and coast of arrival: Two important concepts for the formation and structure of convective snowbands over seas and lakes. *Mon. Wea. Rev.*, **122**, 1036-1049.

Bouteloup, Yves, 1995: Improvement of the Spectral Representation of the Earth Topography with a Variational Method. *Mon. Wea. Rev.*, **123**, 1560-1573.

Davies, H.C., 1976: A lateral boundary formulation for multi-level prediction models. *Quart. J. Roy. Meteor. Soc.*, **102**, 405-418.

Gordon, Charles T., and William F. Stern 1982: A description of the GFDL global spectral model. *Mon. Wea. Rev.*, **110**, 625-644.

Gustafsson, Nils, 1991: The HIRLAM model. *Seminar Proceedings on Numerical Methods in Atmospheric Models. Volume II*, pp 115-146. Available from the European Centre for Medium Range Forecasting, Shinfield Park, Reading, England.

Gustafsson, Nils, 1994: Experience with the HIRLAM model with Eulerian and semi-Lagrangian integration schemes. *HIRLAM 3 Workshop on numerical integration techniques, Oslo, 26-27 January, 1994.* pp 23 -26. Available from SMHI S-60176 Norrköping, Sweden.

Gustafsson, Nils, 1995: The HIRLAM spectral model. To appear as a *HIRLAM Technical Report.* Available from SMHI S-60176 Norrköping, Sweden.

Haugen, J.E., and B. Machenhauer 1993: A spectral limited area formulation with time dependent boundary conditions applied to the shallow water equations. *Mon. Wea. Rev.,* **121**, 2618-2630.

Haugen, J.E., 1993: Parallel tests with the Eulerian and semi-Lagrangian HIRLAM models and comparison with the Norwegian LAM model. *HIRLAM 2 final report,* published as *HIRLAM Technical Report no.* **9**. Available from Jan Erik Haugen, Norwegian Meteorological Institute, P.O. Box 43, Blindern, 0313 Oslo, Norway.

Hortal, M., and A. J. Simmons, 1991: Use of reduced Gaussian grids in spectral models. *Mon. Wea. Rev.,* **119**, 1057-1074.

Jarraud, M., and A.J. Simmons 1984: The spectral technique. *Seminar 1983. Numerical methods for weather prediction.* Available from ECMWF, Shinfield Park, Reading, Berkshire RG2 9AX, England; Volume 2, page 47-54.

Jarraud, M., and C. Girard 1984: An extensive operational comparison between a spectral and a grid point model. *Seminar 1983. Numerical methods for weather prediction.* Available from ECMWF, Shinfield Park, Reading, Berkshire RG2 9AX, England; Volume 2, page 92-112.

Kaas, E., 1987: The construction of and tests with a multi-level semi-Lagrangian and semi-implicit limited area model. *Masters Thesis, University of Copenhagen Geophysical Institute.*

Källberg, Per, 1990: *HIRLAM forecast model level 1 documentation manual.* Available from SMHI S-60176 Norrköping, Sweden; 77 pages.

Machenhauer, B., and Jan Erik Haugen 1987: Test of a spectral limited area shallow water model with time dependent lateral boundary conditions and combined normal mode / semi-Lagrangian time integration schemes. *Workshop proceedings on Techniques for horizontal discretization in numerical prediction models.* Available from ECMWF, Shinfield Park, Reading, Berkshire RG2 9AX, England; 2.1-2.28.

Moorthi, S., Higgins, R.,W., and J.R. Bates 1994: A global multi-level atmospheric model using a vector semi-Lagrangian finite difference scheme. Part 2; version with physics. *Mon. Wea. Rev., to be published*

McDonald, A., and J.E. Haugen, 1992: A two time level, three dimensional semi-Lagrangian, semi-implicit, limited area, grid point model of the primitive equations. *Mon. Wea. Rev.*, **120**, 2603-2621.

McDonald, A., and J.E. Haugen, 1993: A two time level, three dimensional semi-Lagrangian and semi-implicit grid point model II. Extension to hybrid coordinates. *Mon. Wea. Rev.*, **121**, 2077-2087.

McDonald, A., 1994: Using second, fourth, and sixth order implicit horizontal diffusion to control noise in three dimensional semi-Lagrangian, semi-implicit, limited area, grid point models of the primitive equations. *HIRLAM3 Workshop on numerical integration techniques, Oslo, 26-27 January 1994*, p17. Available from Aidan McDonald, Irish Meteorological Service, Glasnevin Hill, Dublin 9, Ireland.

Radnoti, G., 1995: Comments on "A Spectral Limited-Area Formulation with Time-dependent Boundary Conditions Applied to the Shallow-Water Equations". To appear in *Mon. Wea. Rev.*.

Raymond, W.H., 1988: High-order low-pass implicit tangent filters for use in finite area calculations. *Mon. Wea. Rev.*, **116**, 2132-2141.

Ritchie, H., A. Simmons, M. Hortal, T Davies, D. Dent, and M. Hamrud, 1994: Implementation of the semi-Lagrangian method in a high resolution version of the ECMWF forecast model. *Mon. Wea. Rev.*, **123**, 489-514.

Staniforth, A., and J. Coté, 1991: Semi-Lagrangian integration schemes for atmospheric models: a review. *Mon. Wea. Rev.*, **119**, 2206-2223.